J Appl Electrochem (2017) 47:1179–1188
DOI 10.1007/s10800-017-1111-0

RESEARCH ARTICLE

Electrochemical comparison of $LiFePO_4$ synthesized by a solid-state method using either microwave heating or a tube furnace

Cecilia A. Calderón[1] · Jorge E. Thomas[2] · German Lener[1] · Daniel E. Barraco[1] · Arnaldo Visintin[2]

Received: 30 March 2017 / Accepted: 8 August 2017 / Published online: 17 August 2017

Abstract $LiFePO_4$/C composites were successfully prepared by a solid-state reaction in order to compare conventional heat treatment and microwave-assisted synthesis at different times of sintering. Microwave-assisted synthesis is interesting due to the fact that energy and inert gas consumption can be greatly reduced with respect to the conventional treatment, resulting in a cheaper synthesis method. The relationship between particle morphology and crystal structure using the composite synthesis was characterized by scanning electron microscopy (SEM), transmission electron microscopy (TEM), and X-ray diffraction (XRD) with refinements of the crystal structures carried out by the Rietveld method. In addition, the electrochemical performances were evaluated using constant current charge/discharge tests, cyclic voltammetry (CV), and electrochemical impedance spectroscopy (EIS). It was observed that the samples prepared by microwave heating had a better electrochemical behavior than those prepared in a conventional furnace. Also, in general, a higher sintering time improved the electrochemical behavior, but with increased particle sizes, and consequently, a decreased specific capacity.

Electronic supplementary material The online version of this article (doi:10.1007/s10800-017-1111-0) contains supplementary material, which is available to authorized users.

✉ Cecilia A. Calderón
acalderon@famaf.unc.edu.ar

[1] Instituto Enrique Gaviola (IFEG),CCT Córdoba-CONICET, Facultad de Matemática, Astronomía y Física, Universidad Nacional de Córdoba (UNC), Av. Medina Allende s/n, Ciudad Universitaria, 5000 Córdoba, Argentina

[2] Instituto de Investigaciones Fisicoquímicas Teóricas y Aplicadas (INIFTA), Facultad de Ciencias Exactas, CCT La Plata-CONICET, Universidad Nacional de La Plata (UNLP), CC 16, Suc. 4, 1900 La Plata, Argentina

Graphical Abstract

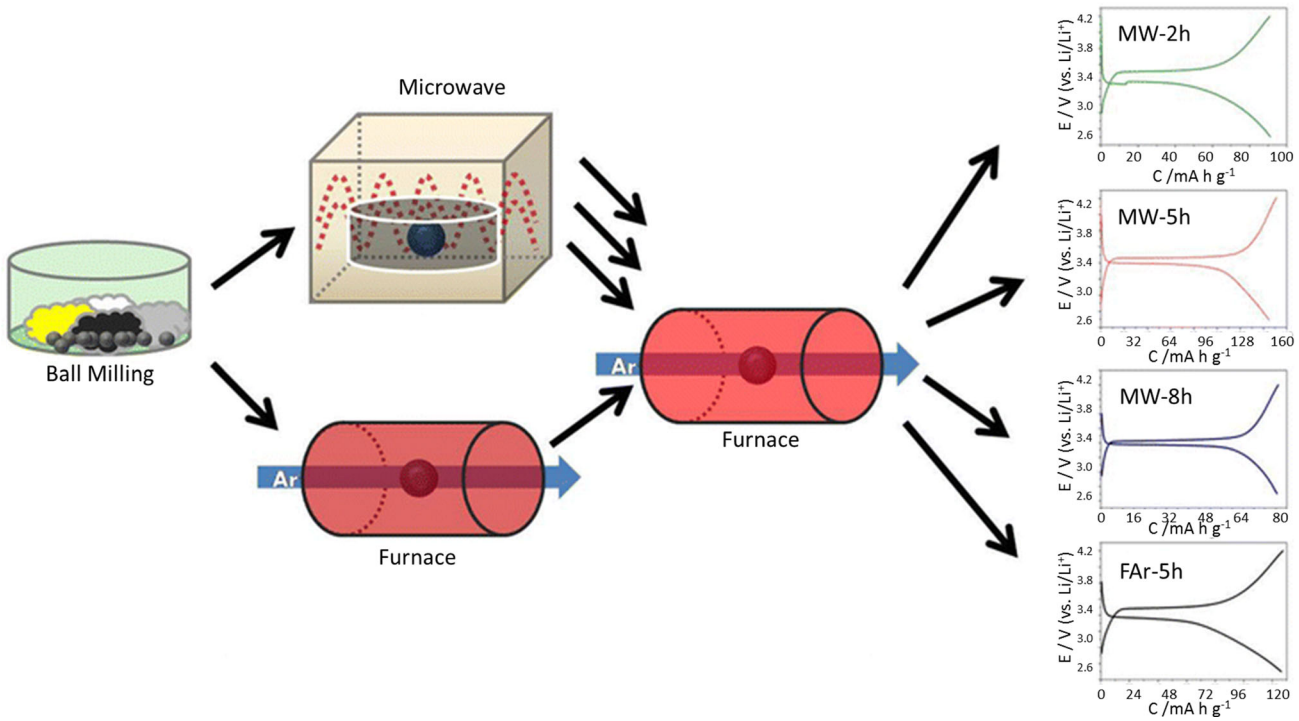

Keywords Lithium-ion battery · Cathode · Lithium iron phosphate · Microwave

1 Introduction

Lithium-ion batteries have been successfully utilized in various portable electronic devices such as mobile phones and laptops [1], and they are currently considered to be ideal candidates for power sources in future electric vehicles [2]. However, this type of battery is made up of various components, and it is still necessary to improve the cathodic and anodic active materials, electrolytes, and separators, among other factors [3]. In this regard, layered $LiCoO_2$ is one of the earliest developed cathode materials, and became the main commercially used cathode material despite its toxicity and high cost. Since the commercialization of $LiCoO_2$ by SONY in 1991, alternative cathode materials have been pursued in order to improve battery performance and reduce costs and the negative environmental effects. Among these materials, $LiFePO_4$ of the olivine family, proposed by Goodenough [4], is recognized as the most attractive candidate to replace $LiCoO_2$ as the cathodic material for lithium-ion batteries, due to its cycling and thermal stability [5], low cost, safety, and low environmental impact. Nevertheless, it still has some drawbacks, including its low capacity and low ionic and electronic conductivities [6].

Some strategies have been investigated with the aim of improving the material behavior, such as making smaller particles, covering the material with a conductive shell such as carbon [7–9], or doping with other metallic ions [10, 11]. The traditional $LiFePO_4$/C synthesis method via the solid phase pathway consists of two heating stages, each of which can take between 5 and 24 h. The first of them is the synthesis step and is carried out at temperatures close to 350 °C, causing the reactants to form $LiFePO_4$/C. Then, a second step (sintering) is performed at temperatures near 800 °C, and here $LiFePO_4$/C forms an ordered crystal structure, with particles agglomerating and increasing in size. During this time, the reactor (usually a furnace) must be working in an inert (or reductive) atmosphere, for example, argon or an argon/hydrogen atmosphere [12]. Due to cost considerations, it is also important to make this procedure cheaper and also faster in order to be practical for its industrial application. However, the synthesis of $LiFePO_4$ is not easily performed because of the iron oxidation state, so it has usually been controlled by heating the furnace with reductive or inert gas flow for several hours, which is not only an expensive procedure (in terms of the energy involved and because of the necessity of using an inert atmosphere), but is also difficult to apply on an industrial scale. One possible way to overcome this issue is through microwave processing, which has been applied in the preparation of many materials and has been used for the successful synthesis of $LiFePO_4$ compounds

[10–14]. In fact, microwave irradiation is highly beneficial for solid-state reactions since substances are heated uniformly at the molecular level, in contrast with conventional heating where samples are heated from the outer surface inwards, resulting in a steep thermal gradient. The basic idea of using microwave-assisted heat treatment here is to make the iron atoms act as a microwave absorber, so that they can heat the precursor and the activated carbon rapidly and form a reductive atmosphere by simultaneous carbon oxidation reactions. In this way, $LiFePO_4$ can be obtained by microwave heating in just a few minutes, thereby avoiding iron oxidation by not using an inert gas flow, which implies that the energy and supply consumption can be greatly reduced, with the whole preparation process being significantly simplified.

In addition to improving the synthesis of $LiFePO_4$, it is necessary to optimize the control of the carbon formed in the composite to improve the electronic and ionic conductivity, and thus maximize the specific capacity and rate capability. This can be achieved using different times and temperatures for the heat treatment of the composite.

In this study, $LiFePO_4$/C was prepared by a solid-state reaction, and during the first step (synthesis) microwave irradiation and a conventional furnace with an inert atmosphere were used to compare methods. These samples were then sintered in an inert atmosphere to obtain the olivine structure, which allows the intercalation of lithium ions. Then, the effects of different sintering times on the characteristics of the obtained materials were studied. All samples were characterized both physically and electrochemically.

2 Experimental

2.1 Material synthesis

$LiFePO_4$/C (LFP/C) was prepared by a solid-state reaction method using iron (II) oxalate ($FeC_2O_4 \bullet 2H_2O$), lithium hydroxide hydrate ($LiOH \bullet H_2O$ 99%), and ammonium dihydrogen phosphate ($NH_4H_2PO_4$ 99%) as starting materials. A stoichiometric amount of FeC_2O_4 and $NH_4H_2PO_4$ with a 10% excess of LiOH was thoroughly milled with Super P carbon in acetone medium using conventional ball milling apparatus with a rotation speed of about 800 rpm for 10 min. After milling, a 20% weight ratio of glycine (99%) was added to act as the reducing agent and as an extra source of carbon [14, 15]. To study the effect of the use of microwave during synthesis, half of the resulting mixture was subjected to the first synthesis step by microwaving in air for 4 min at 800 W, and the other half of the mixture was heated in a tubular furnace in a flowing argon atmosphere at 350 °C for 5 h.

Finally, to study the effect of carbonization as a function of heat treatment, all the samples were sintered at 750 °C under an inert atmosphere (Ar) to prevent the oxidation process. The samples synthesized by microwave and in a normal furnace under Ar are referred to as MW-5 h and FAr-5 h, respectively, with the (−5 h) notation indicating the duration of the sintering step.

In order to optimize the sintering time of microwave synthesis, samples were prepared using sintering times of 2, 5, and 8 h, and referred to as MW-2 h, MW-5 h, and MW-8 h, respectively. All the obtained materials were milled in a ball milling device, and the powder thus obtained was used for physical and electrochemical characterization.

2.2 Material characterization

The X-ray diffraction (XRD) patterns were recorded at room temperature using a PANalytical X′Pert PRO diffractometer (in Bragg–Brentano geometry with Cu-$K\alpha$ radiation). For the structure refinements, the XRD data were collected in the angular range 15−70° in steps of 0.02°, and with a collection time of 10 s per step^{-1}. The refinements of crystal structures from XRD were performed using the Rietveld method [16] with the FULLPROF software [17].

The scanning electron microscopy (SEM) images were obtained in an FE-SEM Zeiss Σigma high resolution microscope, and the energy-dispersive X-ray spectroscopy (EDS) maps were acquired using the same microscope with a JEOL JXA-8230 microprobe. The transmission electron microscopy (TEM) images were obtained in a TEM Jeol 1200 EX II.

The amount of carbon in the samples was determined by placing 100 mg of material in 10 mL 6 M HCl. Both $LiFePO_4$ phases formed as impurities (Li_3PO_4 and Fe_2P) are soluble in acid medium, whereas the carbonaceous compounds are not. Therefore, after mixing, the samples were filtered, washed with Milli-Q water, and dried, and the remaining carbon was weighed [18].

2.3 Electrochemical characterization

The working electrodes were prepared by mixing the active material with Super P carbon and polyvinylidene fluoride (PVDF) in *N*-methyl-2-pyrrolidone (NMP) at a weight ratio of 80:10:10, respectively. The slurry was then coated onto aluminum foil, dried, and pressed to make the electrodes. Swagelok T cells were utilized for the measurements, with metallic Li as the counter and reference electrodes, and fiber glass (MGD grade, pore size 2.7 μm MUNKTELL) as separator. The electrolyte consisted of 1 M $LiPF_6$ in ethylene carbonate/dimethyl carbonate (EC/DMC, volume

ratio 1:1), and the cells were assembled inside a glove box in an Ar atmosphere. All tests were conducted at 25 °C.

Charge/discharge cycles, rate capability, and stability studies were carried out with Arbin MSTAT4 in galvanostat mode between 2.7 and 4.2 V versus Li/Li^+. Cyclic voltammetry and electrochemical impedance spectroscopy studies were performed using an AutoLab PGSTAT302N.

3 Results and Discussion

3.1 Physical characterization

3.1.1 X-ray diffraction

The XRD patterns with Rietveld refinements are shown in Fig. S1. Figure S1a shows a high crystallinity in the case of the precursors treated in a microwave furnace. However, the precursors treated in a conventional furnace for 5 h in Ar at 350 °C show a low crystallinity and weak signals associated with the formation of olivine $LiFePO_4$ phase. The Rietveld refinement of the precursors treated in a microwave furnace is shown in Fig. S1b. The formed crystallographic phases correspond to olivine $LiFePO_4$ (48.2%), Li_3PO_4 (24.7%), Fe (4%), graphite C (11.4%), and cubic C (11.7%). The presence of metallic Fe and structured C indicates the reductive condition of this experimental approach. On the other hand, the presence of cubic carbon would indicate the high pressure induced under this condition. At this synthesis step, a considerable amount of olivine $LiFePO_4$ is formed, and Fe, Li_3PO_4, and C are the precursors for the final composition of the materials obtained at 750 °C at different sintering times.

The XRD patterns of the samples treated at 750 °C at different times can be indexed for three phases: $LiFePO_4$ with a space group Pnma, with an orthorhombic olivine-type structure Fe_2P, and Li_3PO_4 (see Fig. S1c–f; Table 1). The composition of the samples changed with the time of sintering, with the amount of Fe_2P decreasing as the sintering time increased. The sample with the lowest amount of $LiFePO_4$ was FAr-5 h, which also had the highest amount of Fe_2P, a compound that is formed during the synthesis process by carbothermal reduction [19] and apparently favored the materials synthesized in a furnace with respect to those synthesized in a microwave. However, other phases that have been previously reported in materials prepared using microwaves when the environment is not reductive enough, such as $Li_4P_2O_7$ or $Li_3Fe_2(PO_4)_3$, were not found [14].

Table 1 Rietveld quantification of crystalline phases of the different synthesis methods

Sample	% $LiFePO_4$	% Fe_2P	% Li_3PO_4
FAr-5 h	82.5	11.1	6.4
MW-2 h	94.2	3.8	2.0
MW-5 h	87.1	3.1	9.8
MW-8 h	91.2	1.1	7.7

An extra peak at 26.5° was present in the patterns of the synthesized microwave samples, corresponding to a crystalline carbonaceous phase (graphite with the space group rhombohedral R-3 m), indicating that the heat treatment induced the formation of graphitic carbon. The presence of a graphitic structure could have been the determining factor in the increase in the electronic and ionic conductivity, and may have enhanced the charge transfer at the electrode/electrolyte interface. This phase was not included in the Rietveld quantification because it did not appear for FAr-5 h and MW-2 h. Thus, if we had included it, the percentage quantifications would not have been comparable for all the samples as it would have changed the quantification of the $LiFePO_4$, Li_3PO_4, and Fe_2P crystallographic phases. On the other hand, the intensity of the graphite peak depends on the sintering treatment of the materials and consequently, the sample MW-8 h could have had a better graphitization degree than the others. Moreover, the graphitic phase did not appear for FAR-5 h, so some precursor of this carbonaceous phase may have been formed by the microwave treatment, and the formation of the graphitic structure should have occurred when the powder was sintered at 750 °C in Ar flux.

3.1.2 Morphological characterization

Scanning electron micrographs are displayed in Fig. 1, showing that the particle shape is similar for all samples, with small faceted crystallites agglomerated into larger particle groups. By comparing FAr-5 h with MW-5 h, although there are no major significant differences in the particle sizes, MW-5 h has areas with a smoother appearance, which may have been due to the presence of graphitic carbon species. For all samples, as sintering time increased the size of the particles clearly increased too, as reported in the bibliography [20, 21].

X-ray maps for MW-5 h are displayed in Fig. S2, showing that the other sample maps, which are included for comparison purposes, are similar to those observed in MW-5 h. It can be seen that Fe, P, and O are uniformly distributed on the particles, which is consistent with the data obtained by X-ray diffraction, indicating that the sample is composed mainly of $LiFePO_4$. The carbon signal is displayed in Fig. S2f, where it can be noted that there are more signals in the softer areas of the electronic image, coinciding with an amorphous structure of carbonaceous

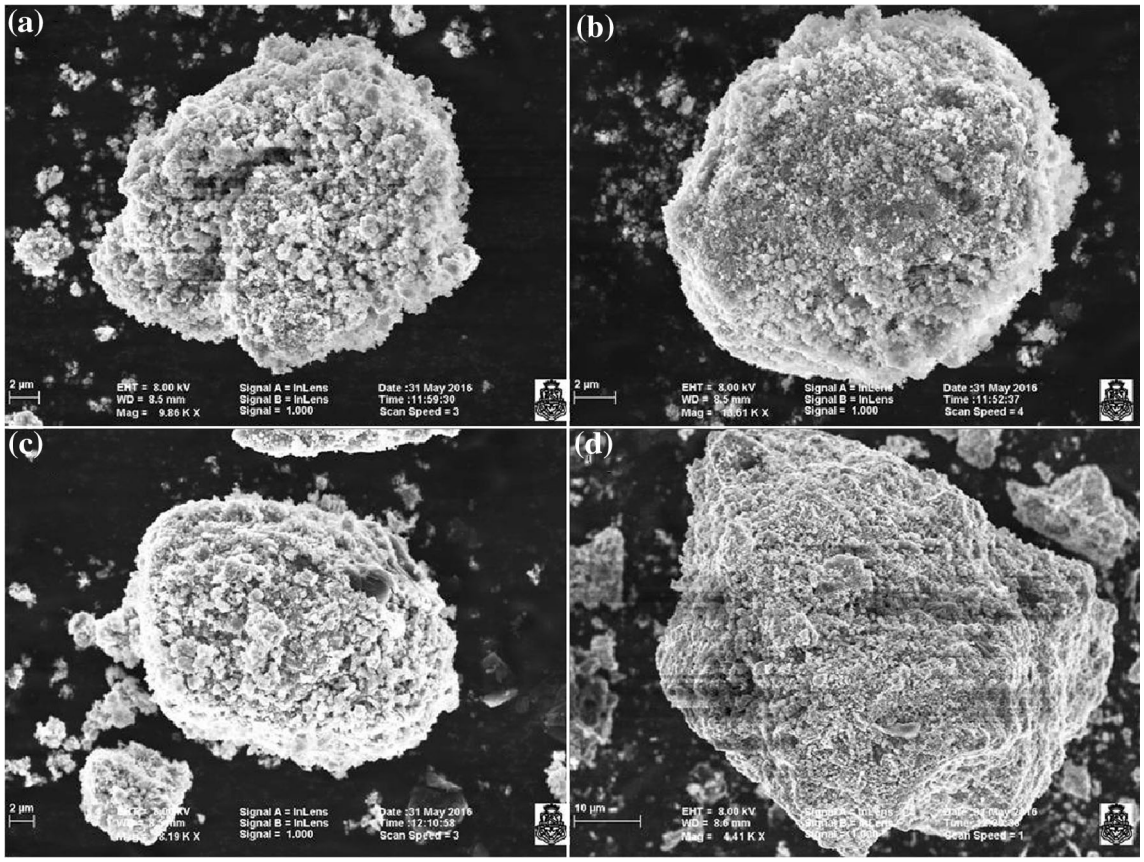

Fig. 1 SEM images of **a** FAr-5 h, **b** MW-2 h, **c** MW-5 h, **d** MW-8 h

materials. In addition, the carbon signal can be observed over the entire surface of the particle.

The TEM images of the samples heated by microwave are shown in Fig. 2. Contour lines have been added to facilitate the observation of the different particulates, which are agglomerated by a carbonaceous matrix. The shapes of these particles are irregular for all samples. Also, as mentioned above, it can be observed that the particle size increased with sintering time, with the measurements recorded being between 70 and 170 nm for MW-2 h, 140 and 220 nm for MW-5 h, and 150 and 560 nm for MW-8 h.

3.2 Electrochemical characterization

The charge–discharge curves at C/2 are shown in Fig. 3, and the capacities obtained (corrected with the percentages of $LiFePO_4$ obtained by the Rietveld method) are given in Table 2. The sample synthesized in the microwave had a higher capacity than its couple synthesized in the furnace. In addition, on comparing the different times of sintering for the microwave-synthesized materials, it can be seen that the material treated for 5 h had the highest capacity.

The potential differences between charge and discharge plateau values are listed in Table 2. With respect to FAr-5 h and MW-5 h, it is clear that the sample synthesized in the furnace showed a bigger potential difference between plateaus. For the microwave-synthesized samples, it is evident that the difference between plates decreased as the sintering time increased, in agreement with the difference found between peaks in the CV profiles (Fig. 4a). In fact, we can use the voltage gap between the discharging and charging voltage plateaus as a parameter of electrode polarization, with a lower value of the voltage gap indicating a smaller degree of electrode polarization and improved kinetics of the active material [22–24].

At potential values very close to the equilibrium ones there are linear current–potential regions, which are characteristic of a rapid or reversible electrochemical system. The charge transfer resistances of $LiFePO_4/FePO_4$ oxidation/reduction can be determined from the slope of the linear current–potential domains [25]. For samples synthesized by microwave, the charge transfer resistance decreased with increasing sintering time (Table 3), so MW-8 h had the lowest charge transfer resistance, and as previously stated, had the highest peak of the graphitic phase. It is known that graphite carbons have a better

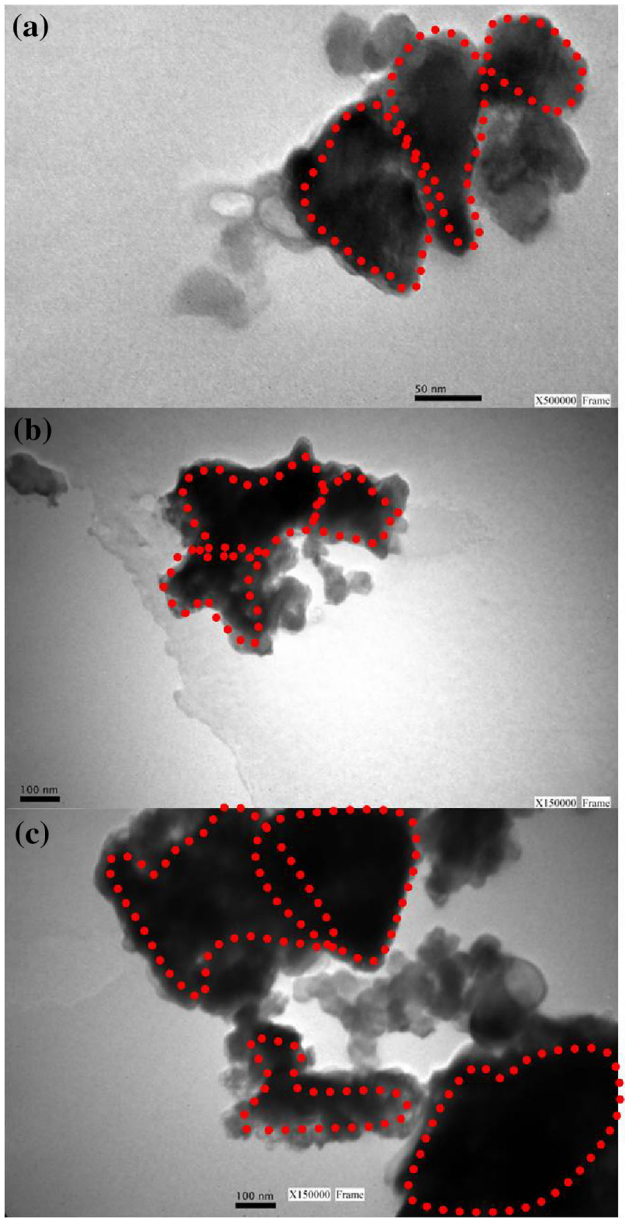

Fig. 2 TEM images of samples **a** MW2 h, **b** MW5 h, and **c** MW8 h

conductivity than amorphous ones, thus the resistance to the transfer of charge was smaller for the sample that had the greatest amount of this type of carbon [26].

In the voltammogram using a 0.1 mV s^{-1} scan rate (Fig. 4), two peaks, corresponding to $LiFePO_4$ oxidation and $FePO_4$ reduction, are centered around 3.42 V versus Li^+/Li, which are characteristic of rapid or reversible electrochemical systems. Cyclic voltammetry was carried out at various scan rates in the range of 0.1–5.0 mV s^{-1} for the different samples to obtain the Li ion diffusivity (Fig. S3), and from the corresponding voltammograms it can be seen that the current peak increased with a rise in the scan rate.

Despite the fact that under the conditions used in this investigation the system was not fully reversible, the ratio of the cathodic to anodic peak was not unity, and the difference between the peak potentials was greater than 59 mV [27] (Table S1), with the peak current being proportional to the square root of the scan rate (Fig. 5). These findings suggest that our electrochemical system is quasi-rapid, and therefore an adapted Randles–Sevcik equation can be used to estimate the apparent diffusion coefficient [28].

For a reaction with only one electron, the Randles–Sevcik equation states that

$$i_p = 0.4463F\left(\frac{F}{RT}\right)^{1/2} C^* v^{1/2} A D^{1/2} \quad (1)$$

where i_p is the peak current (A), F is the Faraday constant (C mol^{-1}), R is the gas constant (J mol^{-1} K^{-1}), T is temperature (K), C^* is the concentration of lithium in the electroactive material (mol cm^{-3}), v is the scan rate (V s^{-1}), A is the electrode area (cm^2), and D is the diffusion coefficient (cm^2 s^{-1}). At 25 °C, Eq. (1) can be rewritten as:

$$\frac{i_p}{m} = 268782\frac{C^{3/2}}{\text{mol.J}^{1/2}} C^* v^{1/2} A D_{\text{app}}^{1/2} \quad (2)$$

Here, D_{app} is the apparent diffusion coefficient because the system is not reversible. $LiFePO_4$ has a bulk density of 3.6 g cm^{-3} with a molar mass of 157.76 g mol^{-1}, corresponding to a Li concentration of 0.0228 mol cm^{-3}. As the Li ions in $LiFePO_4$ were intercalated and de-intercalated along the [010] direction [29, 30], the entire electrode area of parameter A in Eq. (2) was substituted for one-third of the total Brunauer–Emmett–Teller (BET) surface area [31]. Figure 5 shows a linear fit for the samples for both the anodic and cathodic peaks, with the D_{app} values obtained from the slope given in Table 4, which are on the order of those reported in the literature [28, 32, 33]. It can be clearly observed that D_{app} increased with a rise in the sintering time for the samples synthesized by microwave.

Li^+ can move through the material by two forces: external potential or concentration gradient. The mobility of ions represents the degree of ease with which ions pass through media when an external electrical field is applied, and the diffusivity represents the ease with which ions pass through media under a concentration gradient. Diffusivity, mobility, and ionic conductivity are related properties [33], with an increase in the diffusivity or mobility of ions leading to an improvement in the ionic conductivity. Thus, for samples synthesized by microwave, the ionic conductivity improved when the sintering time increased. Furthermore, it can be seen that for the same time of sintering, the sample prepared by microwave

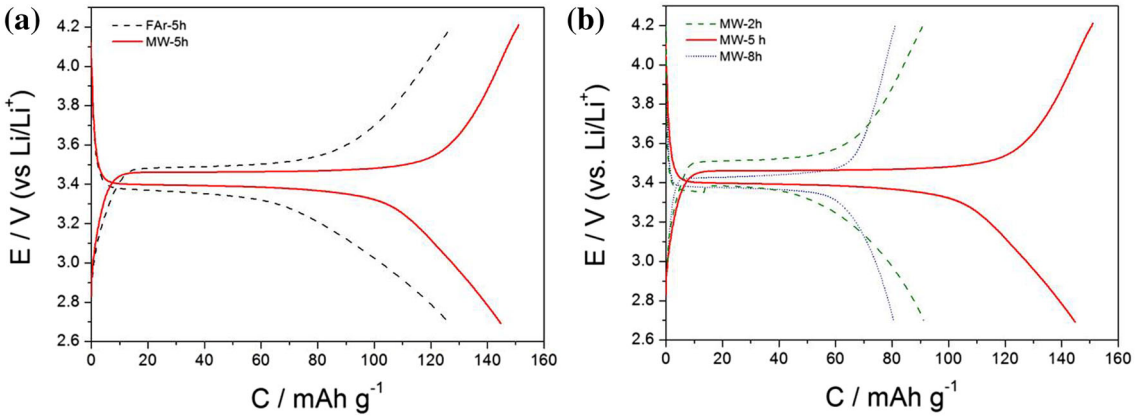

Fig. 3 Charge/discharge profiles of **a** MW-5 h and FAr-5 h, and **b** MW-2 h, MW-5 h, and MW-8 h samples at a rate of 0.5C

Table 2 Capacity potential difference of plateaus and percentage of carbon in the samples

Sample	C/mAh g^{-1}	ΔE/V	% C
MW-2 h	84.4	0.17	8.8
MW-5 h	125.9	0.09	5.2
MW-8 h	72.6	0.08	10.5
FAr-5 h	105.5	0.18	15.2

Table 3 Charge transfer resistance obtained from the slope of the linear current–potential domains in voltammograms measured at 0.1 mV s^{-1} scan rate

Sample	R_{tc}^{ox}/mΩ g	R_{tc}^{red}/mΩ g
MW-2 h	267.4	373.1
MW-5 h	105.8	131.6
MW-8 h	52.6	84
FAr-5 h	172.4	238.1

had a higher ionic conductivity than when synthesized in the furnace.

In Fig. 6 the Nyquist impedance plots are shown. A semicircle can be observed at higher frequencies and a linear response at lower frequencies due to the diffusion of Li^+, which is considered to be the slowest process. At higher frequencies, the time of the perturbation is too short for the diffusion of Li^+ to take place, so the electrode displays a resistive behavior that appears as a semicircle. In contrast, for lower frequencies, as there is enough time for the diffusion process to occur, the Warburg impedance appears. The frequency at the start of the diffusive process (ω_d) increased with sintering time for microwave-synthesized samples, with values of 42, 99, and 148 Hz for MW-2 h, MW-5 h, and MW-8 h, respectively. This indicates that the diffusive mechanism for MW-8 h is quicker than for MW-5 h and in turn faster than for MW-2 h. This is in agreement with the D_{app} tendency discussed above, with a comparison of the ω_d values for MW-5 h and FAr-5 h (33 Hz) also revealing this tendency.

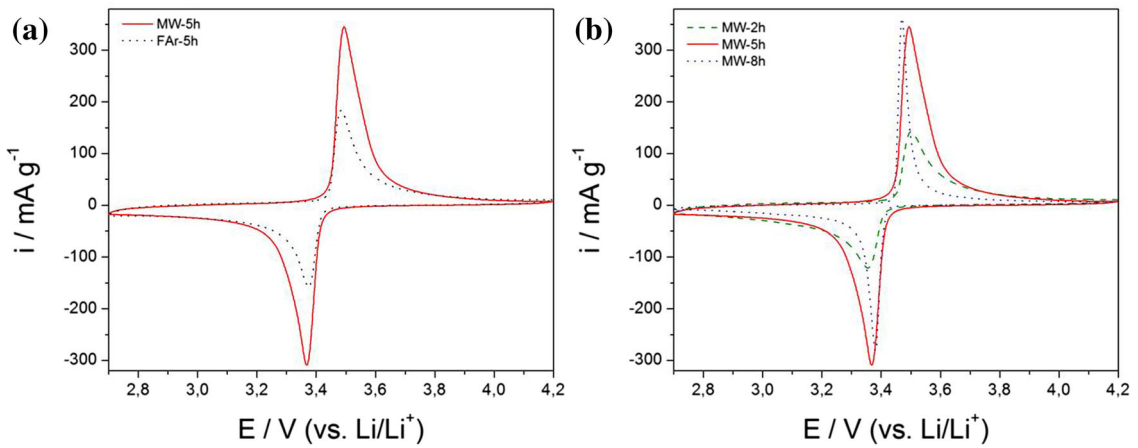

Fig. 4 CV *curves* for comparison of **a** MW-5 h and FAr-5 h, and **b** MW-2 h, MW-5 h, and MW-8 h samples at a 0.1 mV s^{-1} rate

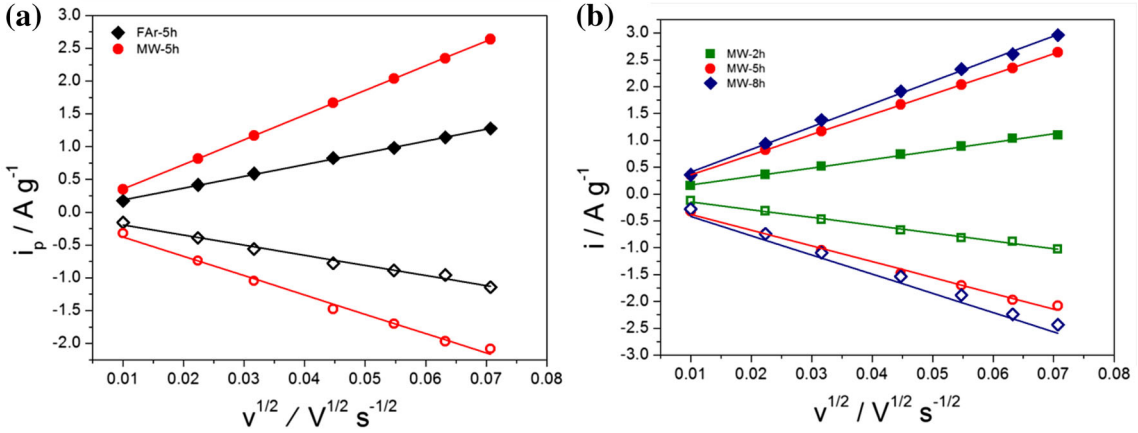

Fig. 5 Normalized peak current versus square root of the scan rate. Comparison of **a** FAr-5 h and MW-5 h, **b** samples heated in a microwave. Lines correspond to a linear fit

Table 4 Apparent diffusion coefficients for anodic and cathodic hemireaction of de-intercalation/intercalation of Li ion, respectively

Sample	D_{app}^{an}/cm^2 s^{-1}	D_{app}^{cat}/cm^2 s^{-1}	$\%\Delta D_{app}$
MW-2 h	2.62×10^{-16}	2.21×10^{-16}	15.9
MW-5 h	1.47×10^{-15}	9.00×10^{-16}	38.5
MW-8 h	1.85×10^{-15}	1.33×10^{-15}	28.2
FAr-5 h	3.35×10^{-16}	2.47×10^{-16}	26.2

The rate capability test results are displayed in Fig. 7, with the response with respect to rate variation being shown in terms of percentage of discharge capacity with respect to maximum capacity. At 5C for example, MW-2 h retained 55% of its initial capacity, while MW-5 h and MW-8 h retained 66 and 78%, respectively. Thus, increasing sintering time clearly improved capacity retention at higher speeds, which is consistent with the improvements in the kinetic properties of the material discussed previously. On comparing microwave and furnace synthesis, it can be seen that the sample synthesized in the microwave had a slightly better retention of its initial capacity at 5C (66% compared with 60%), in agreement with previous findings indicating that MW-5 h has a better kinetic behavior than FAr-5 h (Fig. 7a).

Once the samples had been characterized, we turned our attention to the capacity values (Fig. 3; Table 2). The sample sintered for 8 h had the lowest capacity at C/2, although it was the sample with the best kinetic constants. This may have been because MW-8 h had the biggest particle sizes, which implies that not all the materials were able to intercalate/de-intercalate the Li ions (at the charge/discharge velocity used in the experiments) due to the low diffusion coefficient of Li^+ in $LiFePO_4$.

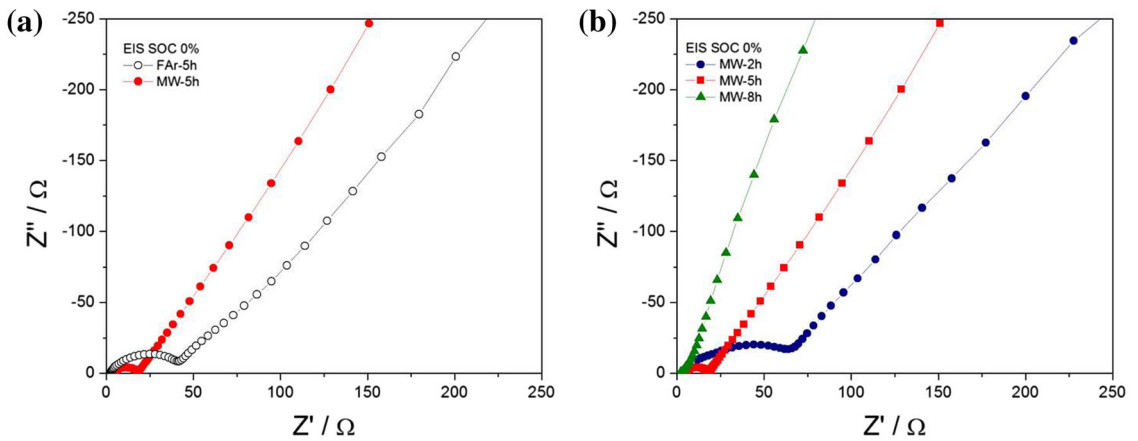

Fig. 6 Nyquist plots of EIS at 0% state of charge. Comparison of **a** FAr-5 h and MW-5 h, and **b** samples heated in a microwave

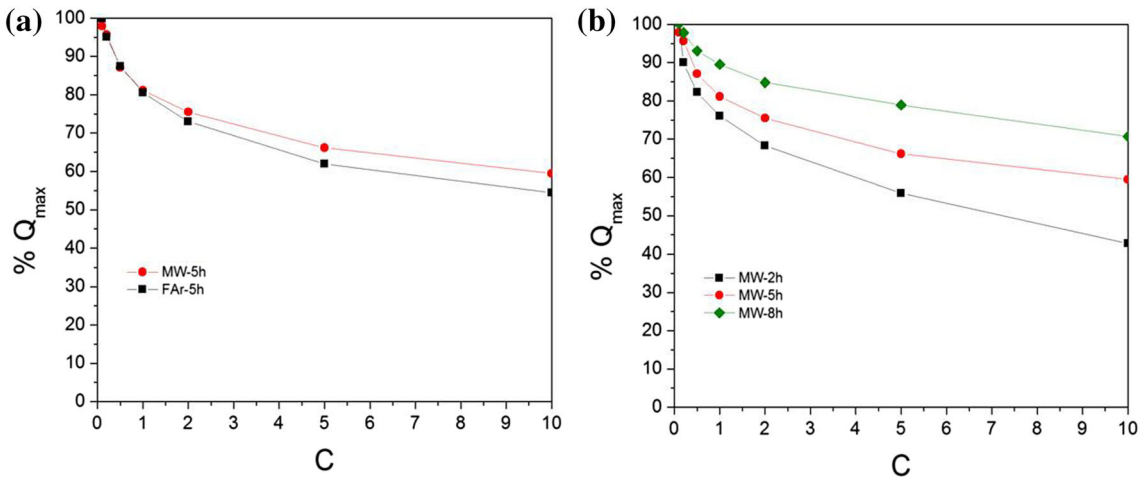

Fig. 7 Comparison of the performance rate of **a** FAr-5 h and MW-5 h, and **b** samples heated in a microwave

4 Conclusions

The $LiFePO_4$/C composite has been synthesized using a solid-state reaction. In order to compare the types of heat treatment, we report on the effects of different types of synthesis and sintering time on the structure, morphology, and electrochemical performance of $LiFePO_4$ using a microwave oven and a conventional furnace. When the microwave was used as the synthesis method, $LiFePO_4$/C had a better electrochemical behavior than when the furnace was used. In addition, a peak of graphitic phase appeared in the X-ray diffraction pattern, whose intensity rose as the sintering time increased. In the case of samples synthesized by microwave, the electrochemical behavior improved considerably with sintering time. The apparent diffusion coefficient for the cathodic reaction was lower for MW-2 h than for MW-5 h, which in turn was lower than that for MW-8 h. This trend is consistent with the other properties studied in this work. However, despite having a better electrochemical behavior, the capacity of MW-8 h was smaller than that of MW-5 h, which may be attributed to the larger particle size preventing the entire active material from participating in the charge/discharge processes at the current rates used in this work.

Acknowledgements We thank the financial support of the "CONICET UE Desarrollo de Baterías de Litio," Argentina. We thank Dr. Paul Hobson, native speaker, for revision of the manuscript.

References

1. Whittingham MS (2004) Lithium batteries and cathode materials. Chem Rev 104:4271–4301. doi:10.1021/cr020731c
2. Zhang WJ (2011) Structure and performance of $LiFePO_4$ cathode materials: a review. J Power Sources 196:2962–2970. doi:10.1016/j.jpowsour.2010.11.113
3. Winter M, Brodd RJ (2004) What are batteries, fuel cells, and supercapacitors ? Chem Rev 104:4245–4270. doi:10.1021/cr020730k
4. Padhi AK, Nanjundaswamy KS, Goodenough JB (1997) Phospho-olivines as positive-electrode materials for rechargeable lithium batteries. J Electrochem Soc 144:1188–1194. doi:10.1684/agr.2014.0700
5. Peng P, Jiang F (2016) Thermal safety of lithium-ion batteries with various cathode materials: a numerical study. Int J Heat Mass Transf 103:1008–1016. doi:10.1016/j.ijheatmasstransfer.2016.07.088
6. Zhou F, Kang K, Maxisch T et al (2004) The electronic structure and band gap of $LiFePO_4$ and $LiMnPO_4$. Solid State Commun 132:181–186. doi:10.1016/j.ssc.2004.07.055
7. Inagaki M (2012) Carbon coating for enhancing the functionalities of materials. Carbon N Y 50:3247–3266. doi:10.1016/j.carbon.2011.11.045
8. Feng J, Wang Y (2016) High-rate and ultralong cycle-life $LiFePO_4$ nanocrystals coated by boron-doped carbon as positive electrode for lithium-ion batteries. Appl Surf Sci 390:481–488. doi:10.1016/j.apsusc.2016.08.066
9. Wang J, Sun X (2015) Olivine $LiFePO_4$: the remaining challenges for future energy storage. Energy Environ Sci 8:1110–1138. doi:10.1039/C4EE04016C
10. Hsieh C-T, Liu J-R, Juang R-S et al (2015) Microwave synthesis of copper network onto lithium iron phosphate cathode materials for improved electrochemical performance. Mater Chem Phys 153:103–109. doi:10.1016/j.matchemphys.2014.12.040
11. Naik A, Zhou J, Gao C et al (2016) Rapid and facile synthesis of Mn doped porous $LiFePO_4$/C from iron carbonyl complex. J Energy Inst 89:21–29. doi:10.1016/j.joei.2015.01.013
12. Jugović D, Uskoković D (2009) A review of recent developments in the synthesis procedures of lithium iron phosphate powders. J Power Sources 190:538–544. doi:10.1016/j.jpowsour.2009.01.074
13. Wang Z, Guo H, Yan P (2014) A rapid microwave heating route to synthesize graphene modified $LiFePO_4$/C nanocomposite for rechargeable lithium-ion batteries. Ceram Int 40:15801–15806. doi:10.1016/j.ceramint.2014.07.106
14. Yu F, Zhang L, Zhu M et al (2014) Overwhelming microwave irradiation assisted synthesis of olivine-structured LiMPO4 (M = Fe, Mn, Co and Ni) for Li-ion batteries. Nano Energy 3:64–79. doi:10.1016/j.nanoen.2013.10.011

15. Wang L, Liang GC, Ou XQ et al (2009) Effect of synthesis temperature on the properties of $LiFePO_4$/C composites prepared by carbothermal reduction. J Power Sources 189:423–428. doi:10.1016/j.jpowsour.2008.07.032
16. Rietveld HM (1969) A profile refinement method for nuclear and magnetic structures. J Appl Crystallogr 2:65–71. doi:10.1107/S0021889869006558
17. Rodríguez-Carvajal J (1993) Recent advances in magnetic structure determination by neutron powder diffraction. Phys B Condens Matter 192:55–69. doi:10.1016/0921-4526(93)90108-I
18. Zhu Y, Tang S, Shi H, Hu H (2014) Synthesis of $FePO_4 \bullet \times H_2O$ for fabricating submicrometer structured $LiFePO_4$/C by a co-precipitation method. Ceram Int 40:2685–2690. doi:10.1016/j.ceramint.2013.10.055
19. Kim CW, Lee MH, Jeong WT, Lee KS (2005) Synthesis of olivine $LiFePO_4$ cathode materials by mechanical alloying using iron(III) raw material. J Power Sources 146:534–538. doi:10.1016/j.jpowsour.2005.03.058
20. Kim CW, Park JS, Lee KS (2006) Effect of Fe_2P on the electron conductivity and electrochemical performance of $LiFePO_4$ synthesized by mechanical alloying using Fe^{3+} raw material. J Power Sources 163:144–150. doi:10.1016/j.jpowsour.2006.02.071
21. Yamada A, Chung SC, Hinokuma K (2001) Optimized $LiFePO_4$ for lithium battery cathodes. J Electrochem Soc 148:A224–A229. doi:10.1149/1.1348257
22. Hu YS, Guo YG, Dominko R et al (2007) Improved electrode performance of porous $LiFePO_4$ using RuO_2 as an oxidic nanoscale interconnect. Adv Mater 19:1963–1966. doi:10.1002/adma.200700697
23. Yu F, Zhang J, Yang Y, Song G (2010) Porous micro-spherical aggregates of $LiFePO_4$/C nanocomposites: a novel and simple template-free concept and synthesis via sol-gel-spray drying method. J Power Sources 195:6873–6878. doi:10.1016/j.jpowsour.2010.01.042
24. Zhang M, Liu R, Feng F et al (2015) Etching preparation of (010)-defective $LiFePO_4$ platelets to visualize the one-dimensional migration of Li^+ ions. J Phys Chem C 119:12149–12156. doi:10.1021/acs.jpcc.5b02270
25. Delacourt C, Laffont L, Bouchet R et al (2005) Toward understanding of electrical limitations (electronic, ionic) in $LiMPO_4$ (M = Fe, Mn) electrode materials. J Electrochem Soc 152:A913. doi:10.1149/1.1884787
26. Wang J, Sun X (2012) Understanding and recent development of carbon coating on $LiFePO_4$ cathode materials for lithium-ion batteries. Energy Environ Sci 5:5163–5185. doi:10.1039/C1EE01263K
27. Bard AJ, Faulkner LR, York N et al (1944) Electrochemical methods fundamentals and applications. Electrochem I Faulkner, Larry R. doi:10.1016/B978-0-12-381373-2.00056-9
28. Yu DYW, Fietzek C, Weydanz W et al (2007) Study of $LiFePO_4$ by cyclic voltammetry. J Electrochem Soc 154:A253. doi:10.1149/1.2434687
29. Morgan D, Van der Ven A, Ceder G (2004) Li conductivity in Li_xMPO_4 (M = Mn, Fe Co, Ni) olivine materials. Electrochem Solid-State Lett 7:A30. doi:10.1149/1.1633511
30. Ouyang C, Shi S, Wang Z et al (2004) First-principles study of Li ion diffusion in $LiFePO_4$. Phys Rev B 69:104303. doi:10.1103/PhysRevB.69.104303
31. Park CK, Bin Park S, Oh SH et al (2011) Li ion diffusivity and improved electrochemical performances of the carbon coated $LiFePO_4$. Bull Korean Chem Soc 32:836–840. doi:10.5012/bkcs.2011.32.3.836
32. Prosini PP, Lisi M, Zane D, Pasquali M (2002) Determination of the chemical diffusion coefficient of lithium in $LiFePO_4$. Solid State Ionics 148:45–51. doi:10.1016/S0167-2738(02)00134-0
33. Park M, Zhang X, Chung M et al (2010) A review of conduction phenomena in Li-ion batteries. J Power Sources 195:7904–7929. doi:10.1016/j.jpowsour.2010.06.060